Colloids and Surfaces A: Physicochem. Eng. Aspects 470 (2015) 258–267

Contents lists available at ScienceDirect

Colloids and Surfaces A: Physicochemical and Engineering Aspects

journal homepage: www.elsevier.com/locate/colsurfa

A novel conversion process for waste residue: Synthesis of zeolite from electrolytic manganese residue and its application to the removal of heavy metals

Changxin Li, Hong Zhong*, Shuai Wang*, Jianrong Xue, Zhenyu Zhang

College of Chemistry and Chemical Engineering, Central South University, Changsha 410083, China

HIGHLIGHTS

- A novel conversion process for the utilization of EMR was first proposed.
- Effect of Si/Al ratio on the EMRZ synthesis was investigated.
- EMRZ showed good adsorption properties for removal of Mn^{2+} and Ni^{2+} ions.
- The adsorption mechanism and kinetics were systematically studied.
- Ion exchange was responsible for metal ions removal.

GRAPHICAL ABSTRACT

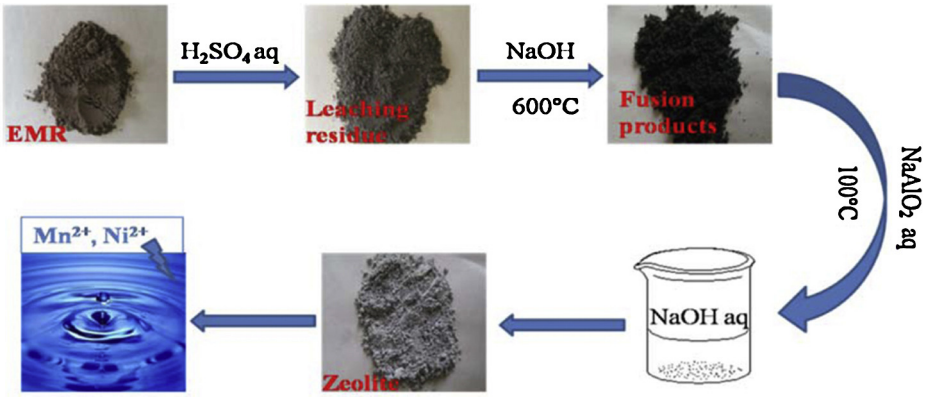

ARTICLE INFO

Article history:
Received 1 November 2014
Received in revised form 29 January 2015
Accepted 2 February 2015
Available online 9 February 2015

Keywords:
Electrolytic manganese residue
Zeolite
Heavy metal
Removal
Kinetics

ABSTRACT

The zeolite material was first synthesized from electrolytic manganese residue (EMRZ), by a two-step synthetic procedure using NaOH and $NaAlO_2$ within a short aging period. Based on the detailed analyses using XRD, FT-IR, FE-SEM, XRF, CEC and BET surface area measurement, the product synthesized at Si/Al ratio = 1.5 was mainly composed of Na-A zeolite with a specific surface area of 35.38 $m^2\ g^{-1}$. Then, the removal characteristics of Mn^{2+} and Ni^{2+} ions by EMRZ were investigated under various operating variables like contact time, solution pH and initial metal concentration. The adsorption equilibrium for both Mn^{2+} and Ni^{2+} was best described by the Langmuir model, confirming the applicability of monolayer coverage of metal ions onto EMRZ particles. The maximum sorption capacities for Mn^{2+} and Ni^{2+} shown by EMRZ were 66.93 mg g^{-1} and 128.70 mg g^{-1}, respectively. It was also found that adsorption of Mn^{2+} and Ni^{2+} by EMRZ followed second-order kinetics and rate constants for Mn^{2+} and Ni^{2+} sorption were found to be 0.001091 and 0.005668 g mg^{-1} min^{-1}, respectively at 30 °C. These results indicate that the synthesized EMRZ is a promising and low-cost adsorbent for removing heavy metals from wastewater due to higher adsorption capacity than other adsorbents.

1. Introduction

Rapid industrialization has led to increased disposal of heavy metals into the environment, causing serious soil and water pollution [1]. Meanwhile, heavy metals are not biodegradable and tend

* Corresponding authors. Tel.: +86 731 88830654.
E-mail addresses: zhongh@csu.edu.cn (H. Zhong), wangshuai@csu.edu.cn (S. Wang).

http://dx.doi.org/10.1016/j.colsurfa.2015.02.003
0927-7757/

to accumulate in living organisms causing various diseases and disorders [2,3]. Moreover, heavy metals are priority toxic pollutants that severely limit the beneficial use of water for domestic or industrial applications. Thus considerable attention has been paid to methods for metal removal from industrial wastewaters as the global interests in this issue increase over the past decades [3–5].

To date, numerous processes exist for removing dissolved heavy metals, including ion exchange, precipitation, phytoextraction, ultrafiltration, reverse osmosis, and electrodialysis [6]. Among them, ion exchange techniques using solid adsorbents has been a promising method for treating wastewater, owing to its advantages such as operational simplicity, low cost, availability in large amount and ability to treat pollutants in a sufficiently large scale operation [6,7]. Activated carbon adsorption is considered to be a particularly competitive and effective process for the removal of heavy metals [8]; however, the use of activated carbon is not suitable in developing countries due to the high costs associated with production and regeneration of spent carbon. Consequently, the use of alternative low-cost materials as potential sorbents for the removal of heavy metals has been emphasized recently.

Electrolytic manganese residue (EMR) is a potentially harmful industrial solid waste that comes from the electrolytic manganese industry and has rarely been recycled in large quantities [9]. In the electrolytic manganese metal (EMM) industry, about 6∼9 tons of EMR is discharged into the environment per ton of produced EMM [10]. The common practice in China is collecting the EMR in open sites near the plants. It is highly questionable if the EMR generated is managed properly. Because EMR contains some heavy metal elements and compounds, the untreated discharge can cause serious pollution of surrounding soil and receiving water bodies [11,12]. Additionally, high volume EMR resulting from large scale industrial activities have long been considered to be a burden, due to the high costs for their associated post-treatment, storage and disposal [10,11]. Owing to its mineral composition, EMR has been mostly recycled as hydraulic cement, concrete aggregate, road base, brickmaking materials in civil engineering work, as well as for the production of chemical fertilizers in agricultural work [13–16]. Yet, problems associated with above disposal, such as the potential environmental impacts and the severe environmental regulations, make the recycling of slag difficult. It is, therefore, essential to continuously develop new and advanced recycling processes of EMR.

Recently, our research group found that zeolite can be synthesized using EMR as Si and Al sources. Zeolites are known as ion-exchange materials where the indigenous charge-balancing cations (typically sodium and calcium) are not rigidly fixed to the hydrated aluminosilicate framework and are readily exchanged with metal cations in solution [6,17]. Meanwhile, the fact that zeolite exchangeable ions are relatively innocuous (sodium, calcium, and potassium ions) makes them particularly suitable for removing undesirable heavy metal ions from wastewaters [17,18]. Moreover, zeolites can transfer a heavy metal contamination problem of many thousands of liters to a few kilos of easily handled solid. The toxic metals are firmly held in the crystal structure and do not leach, however for ultimate environmental protection the solid zeolite can be cement stabilized or vitrified [2]. Given these advantages, zeolites (including natural, commercial, and chemically synthesized zeolites) have been intensively studied recently for the removal of heavy metals [17–19]. Accordingly, making use of EMRZ to remove heavy metals can not only reduce the cost, but also comply with the requirement of green economy.

The objective of the present study was to propose a novel conversion process of EMR to zeolite in order to make full use of the economic potential of EMR, and to find out its potential use as low-cost adsorbent for the removal of heavy metals from aqueous solution. Mn^{2+} and Ni^{2+} ions were chosen as a target contaminant to characterize the adsorptive properties of the synthesized zeolite. For the present study, the uptake of heavy metals on EMRZ was evaluated as a function of initial metal ions concentration, pH, and contact time. Further, models to fit the adsorption equilibrium and kinetic data were presented to understand the adsorption mechanism.

2. Materials and methods

2.1. Materials

The EMR investigated in this study was mainly generated in leaching process of the manganese ore (with part of residue generated in electrolytic cell process) at an electrolytic manganese company, situated in western of Hunan province, China. The chemical composition of EMR used in this study is listed in Table 1. This chemical composition is fairly common in EMR produced in China's EMM industry.

Stock solutions of Mn^{2+} and Ni^{2+} ions with concentration at 1000 mg L^{-1} were prepared by dissolving given amounts of $MnSO_4{\cdot}H_2O$ and $Ni(NO_3)_2{\cdot}6H_2O$, respectively, in distilled water. The solutions of different concentrations used in various experiments were obtained by dilution of the stock solutions.

2.2. Zeolite synthesis

The fabrication process of EMRZ is shown in Fig. 1. Based on our previous related studies [20], a fusion method, involving alkaline fusion followed by hydrothermal treatment, was adopted for the synthesis of zeolite in this research. During the hydrothermal reaction process, various amounts of sodium aluminate ($NaAlO_2$) were added into the reaction system to investigate the effect of the ratio of Si/Al. At the end of the process the solid phase was collected by filtration, washed several times with distilled water, and then dried at 100 °C. The obtained samples were labeled based on their initial Si/Al ratios. Namely, the samples with initial Si/Al ratio of 1.5, 2.0 and 2.5 were labeled as EMRZ15, EMRZ20 and EMRZ25, respectively.

2.3. Adsorption studies

The adsorption of heavy metals was performed by shaking 0.3 g of adsorbents with a 100 mL solution of known solute (Mn^{2+} and Ni^{2+} ions) concentration ranging from 100 to 600 mg L^{-1} at 200 rpm in a constant temperature shaker bath. A portion of the solution was collected at predetermined time intervals for kinetics and at equilibrium time for isotherms. The residual concentration was centrifuged at 5000 rpm for 2 min and then determined in triplicate using Thermo SOLAAR atomic absorption spectrophotometers (Thermo Electron, USA). The equilibrium adsorption capacity q_e (mg g^{-1}) was calculated using the following equation.

$$q_e = \frac{(C_0 - C_e)V}{m} \quad (1)$$

where C_0 and C_e (mg L^{-1}) are the concentration of the test solution at the initial stage and under equilibrium conditions, respectively. V (L) is the volume of the test solution and m (g) is the mass of the adsorbent used.

To determine the effect of experimental parameters such as pH and contact time on adsorption process, this method was also applied by varying the corresponding condition. The pH of solution investigated was changed between 1.0 and 6.0 using 0.5 mol/L HCl solutions.

2.4. Characterization

The crystal phase was identified by XRD (D8 Discover, Bruker, Germany). Chemical analysis of EMR, leaching residue and EMRZ

Table 1
Major chemical composition in EMR.

Constituent	Na_2O	SiO_2	Al_2O_3	MgO	K_2O	CaO	MnO	Fe_2O_3	TiO_2
Mass (wt%)	2.7	24.6	12.2	1.7	2.4	8.6	4.6	7.9	0.4

were carried out using an XRF spectroscopy (Axios, PANalytical, Holland). The morphology and particle size of the crystals were observed by field emission scanning electron microscopy (FE-SEM) (Mira3, Tescan, Czech Republic). The furrier transform infra-red spectra (FT-IR) were recorded on a Thermo Scientific Nicolet 6700 FT-IR spectrophotometer. The specific surface area (SSA) was determined by the nitrogen adsorption method. Nitrogen sorption experiments carried out at 77 K using ASAP2020 (Micromeritics, USA). The BET equation was applied to determine the specific surface area. Cation exchange capacity (CEC) of synthesized zeolite was measured according to the study of Zhang et al. [21] and the CEC was calculated and denoted as meq per gram of adsorbents. The pH value of solutions was measured by a pH meter (pHS-3C, Leici, China) with a combination electrode (E-201-C, Leici, China).

3. Results and discussion

3.1. Synthetic procedure of EMRZ and its characterization

3.1.1. Mineralogical composition

In present study, effect of Si/Al ratios on zeolite synthesis was investigated by changing the Si/Al ratio of starting mixture from 1.5 to 2.5 in the three synthesized samples of EMRZ15∼EMRZ25. Fig. 2 shows the XRD patterns of synthesized zeolites, together with leaching residue as a silica source of zeolites. As shown in Fig. 2, the XRD patterns of synthesized samples of EMRZ15∼EMRZ25, exhibit several sharp diffraction peaks, which are different from those present in the untreated leaching residue. Although EMRZ15 showed a detectable diffraction peak for zeolite P (see Fig. 2), no other zeolitic phases, quartz or hydroxysodalite with low porosity were identified. That is to say, the zeolite synthesized at Si/Al ratio = 1.5, namely EMRZ15, was mainly composed of Na-A zeolite. Generally, zeolite with lower Si/Al ratio, i.e. larger Al_2O_3 content, shows higher CEC and adsorption capacity due to the presence of exchangeable cations, which are trapped at the tetrahedral aluminum sites for charge compensation. For this reason, zeolite A, whose Si/Al ratio is inherently quite low, has been widely used as useful cation-exchangers and adsorbents [22–24]. On the other hand, the EMRZ15 synthesized from leaching residue exhibited remarkable diffraction peaks attributable to A-type zeolite, proving that the leaching residue is available enough as a silica source on zeolitie synthesis. These patterns further indicated that the crystallinity and phase purity of synthesized samples are decreased with increasing Si/Al ratio from 1.5 to 2.5.

3.1.2. Chemical composition

Meanwhile, a detailed analysis of chemical composition of EMRZ samples was performed by XRF measurement and the results are summarized in Table 2. As shown in Table 2, small amounts of impurity elements, such as Mg, Fe and Mn, were commonly detected in the zeolites synthesized from the leaching residue. As no detectable peaks attributable to Fe, Mg and Mn compounds were observed in the XRD patterns, it is speculated that those minor metal ions are uniformly dispersed within the structure of EMRZ by replacing the Na^+ sites [23,25]. Meanwhile, the initial Si/Al ratios of 1.5, 2.0 and 2.5 afforded EMRZ15 with Si/Al = 1.01, EMRZ20 with Si/Al = 1.09 and EMRZ25 with Si/Al = 1.17 respectively. It is intriguing to note that the Si/Al ratio of the final product is less than that of the starting reaction mixture. And the explanation is displayed as below. In the experimental conditions adopted in this work, the zeolite A and P with low Si/Al ratio was synthesized from leaching residue (see Fig. 2). Hence, the lower Si/Al ratio of the final product compared to the starting reaction mixture was due to the formation of Al rich zeolite (zeolite A or P). Namely, after the nucleation of zeolite A or P, Al species were consumed more rapidly than Si in the solution [26]. It is well known that Al is the controlling species in the synthesis of zeolites. And almost all Al was depleted during the synthesis of zeolites, however, the extra water-soluble silicates extracted from the starting reaction mixtures was swept away by distilled water in the zeolite synthesis process [27]. Moreover, increasing of Na_2O content of the final product up to 18.7% (taking EMRZ15 for example), in comparison to the leaching residue, which was only 0.1%, is a very clear and promising evidence of CEC improvement in the final product. The remarkable changes in Na_2O content can be considered another evidence of successful conversion [28].

3.1.3. Results of BET surface area measurements

BET surface area measurement was adopted to determine the SSA of the synthesized EMRZ. And the results were shown in Table 3. As shown in Table 3, the SSA of EMRZ15∼EMRZ25 were estimated to be 35.38, 28.64 and 24.13 $m^2 g^{-1}$, respectively. Although the zeolitization process led to an increase in SSA and pore volume

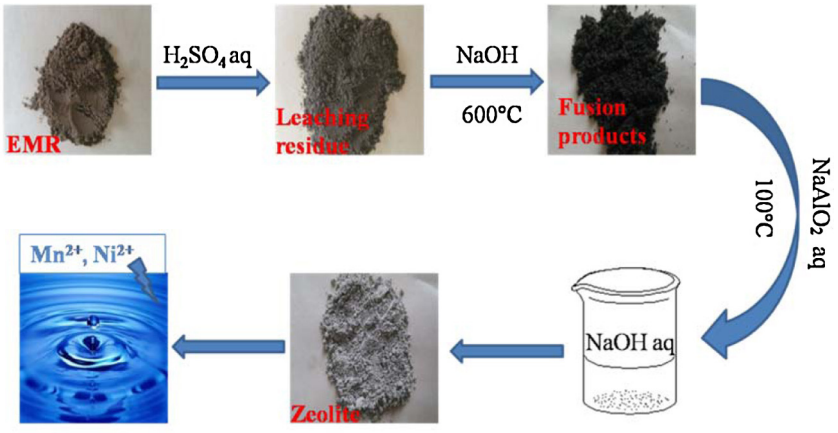

Fig. 1. Schematic illustration of the fabrication procedure of EMRZ.

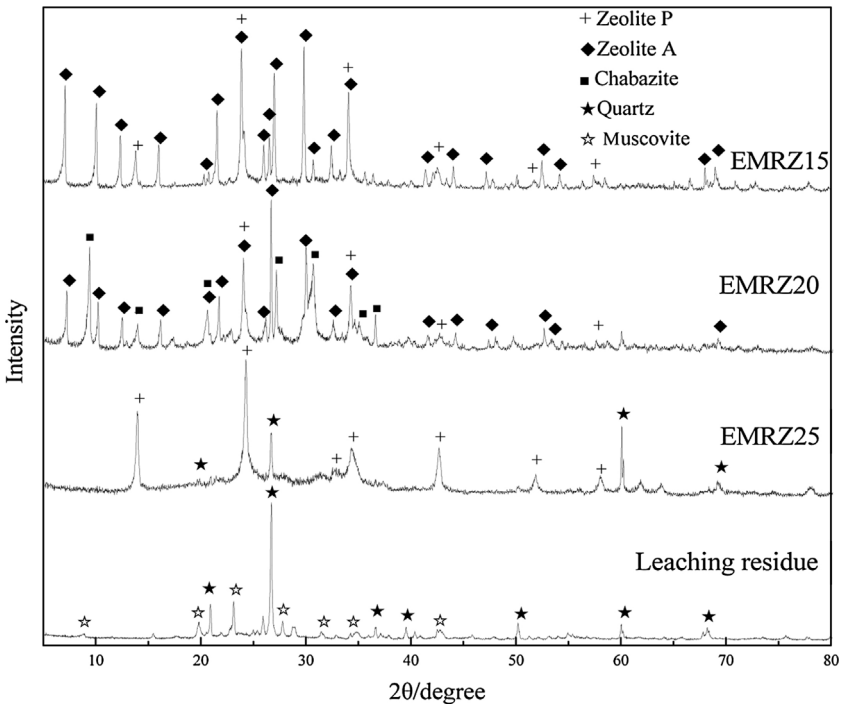

Fig. 2. XRD patterns of samples EMRZ15, EMRZ20, EMRZ25 and leaching residue.

Table 2
The results of elemental analysis of zeolites synthesized from leaching residue.

Sample	Si/Al ratio (starting reaction mixture)	Chemical composition/wt%						Si/Al ratio (final product)
		SiO_2	Al_2O_3	Na_2O	Fe_2O_3	MgO	MnO	
EMRZ15	1.5	35.1	29.5	18.7	0.76	0.24	0.13	1.01
EMRZ20	2.0	35.4	27.5	16.8	0.87	0.27	0.15	1.09
EMRZ25	2.5	35.5	25.7	15.1	0.92	0.25	0.17	1.17
Leaching residue	3.6	66.4	15.8	0.10	1.1	0.7	0.3	3.60

over the starting material, particularly for EMRZ15 obtained by the fusion method, the obtained values of SSA of EMRZ were much lower than those of commercial or traditional zeolite reported in literatures as expected. However, the efficient utilization of EMR as ingredients of other materials may be advantageous in reduction of not only waste generation but also manufacturing costs. And low SSA of the zeolite synthesized from EMR may be attributed to the low crystallinity of the samples [29]. On the other hand, in particular, the cations or/and impurities in the leaching residue (e.g. Mg, Mn, Fe, etc.) led to a lower surface area than alkali metals (K, Li) did. These results may correlate with pore filling by large cations or partial fusion of the cation compounds during the thermal treatment [30,31].

3.1.4. Results of cation exchange capacity (CEC)

In order to evaluate the ion exchange capability of the as-synthesized zeolite samples, CECs of the zeolites were measured. In Table 4, the CECs of the prepared zeolites are compared with the leaching residue, and some other relevant zeolites in the literatures [21,32–35]. The results obtained revealed that the applied zeolitization process increased the CEC of the EMRZ15~EMRZ25 to 2.15, 1.84 and 1.38 meq/g, respectively. In comparison to zeolite reported in the literatures, EMRZ15 had a higher CEC. This may be caused by fact that low Si/Al ratio and high phase purity of EMRZ15 is synthesized on the basis of fusion method. Moreover, the high CEC value of EMRZ15 was an evidence of high potential for removing ammonium and heavy metals from aqueous solutions [32–35].

Therefore, given the above analysis including XRD, XRF, BET and CECs, a precise control of the synthesis Si/Al ratio in this process drastically alters the composition, type and property of the final product, and that the most suitable Si/Al ratio for the synthesis of EMRZ from leaching residue is 1.5. Therefore, the zeolite synthesized at Si/Al ratio = 1.5 was employed in the heavy metal removal process as shown in Section 3.2.

Table 3
The result of structural parameters of zeolites synthesized from leaching residue.

Sample	Structural parameters	
	SSA/$m^2\ g^{-1}$	V_{BET}/$cm^3\ g^{-1}$
EMRZ15	35.38	0.23
EMRZ20	28.64	0.21
EMRZ25	24.13	0.18
Leaching residue	0.28	0.023

3.1.5. FT-IR spectrometry analysis

Furrier transform infra-red spectroscopy (FT-IR) is a powerful technique for structural characterization of organic and inorganic materials. Hence, FT-IR analysis was determined for sample EMRZ15, as being the best sample of this research shown in Fig. 3. The IR band at 870 cm^{-1}, which can be assigned to T–OH bond in the amorphous precursor of zeolite A, was not observed in Fig. 3 elucidating the successful formation of EMRZ. Because this band disappears as the sample became more crystalline [36]. The band at 1001 cm^{-1} that corresponded to T–O–T (T = Si or Al in zeolite and T is tetrahedrally coordinated) was sharp again signifying that

Table 4
Cation exchange capacity (CEC) of the as-synthesized zeolites in comparison to some related typical zeolites.

Adsorbent	Raw material	CEC/(meq/g)	Reference
EMRZ15	Leaching residue from EMR	2.75	This work
EMRZ20	Leaching residue from EMR	2.04	This work
EMRZ25	Leaching residue from EMR	1.38	This work
Leaching residue	EMR	0.015	This work
Zeolite X	Coal fly ash	2.79	[21]
Zeolite A (Na)	Coal fly ash	0.87∼1.05	[32]
Na-P1	Coal fly ash	0.99∼1.31	[33]
Natural Turkish clinoptilolite	Natural zeolite	0.95∼1.40	[34]
Natural Chinese (Chende) zeolite	Natural zeolite	0.82	[35]

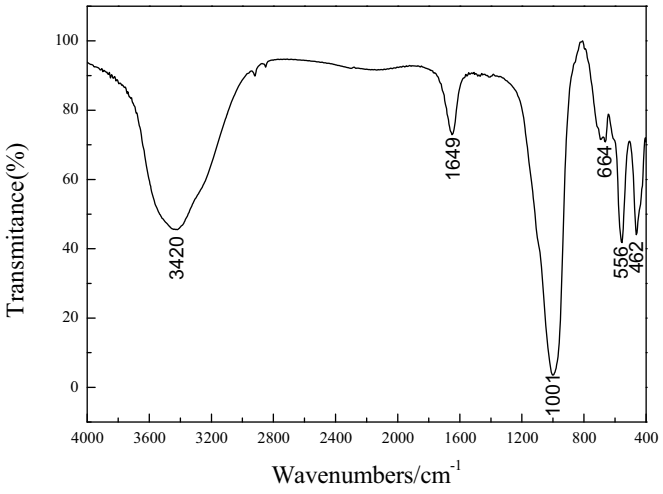

Fig. 3. FT-IR spectra of EMRZ15 in the wave number range of 400 ∼ 4000 cm^{-1}.

the amorphous material was transformed into crystalline zeolite A. The band at 556 cm^{-1} is related to the presence of the double ring (D4R) that is characteristic in the zeolite A [37,38]. The IR bands at 462 and 664 cm^{-1} are assigned to the internal linkage vibrations of the TO_4 tetrahedra and to the asymmetric stretching, respectively, of zeolite A. The band at 1640 cm^{-1} has been associated with the characteristic H–O bending mode of water molecules. Moreover, the observed single strong band at 3420 cm^{-1} was ascribed to the presence of hydroxyls in the sodalite cages as the building blocks of zeolite A. Ultimately, the intensities of these adsorption bands are proportionate to purity of samples and are in agreement with the interpretation of obtained XRD results.

3.1.6. SEM analysis

The morphology and particle size of EMRZ synthesized under optimal conditions (at Si/Al ratio 1.5) were observed by FE-SEM (Fig. 4). The cubic particles with a chamfered shape, along with a small fraction of round crystals were observed in the Fig. 4a. And the cubic and round crystals corresponded to zeolite A and zeolite P, respectively [21,36], which also confirmed by the XRD data in Fig. 2. Meanwhile, the crystal morphology of EMRZ15 with an average size of 1 μm approximately was more clearly shown in Fig. 4b. Besides, it is worth to note that no aggregates were observed in the SEM pictures which indicate that this shape transformation can provide large surface area with tiny pores.

3.2. Removal of heavy metal by EMRZ material

3.2.1. Effect of contact time

Before performing the batch uptake equilibrium experiments, it was necessary to determine the contact time required for adsorption equilibrium. The adsorption of Mn^{2+} and Ni^{2+} onto EMRZ synthesized under optimal conditions, namely EMRZ15, as a function of contact time was studied at 30 °C by varying the contact time from 20 to 300 min while keeping all other parameters constant. The results are shown in Fig. 5. From the Fig. 5, it is shown that the adsorption of the studied heavy metal ions is increased firstly and then kept increasing gradually until the equilibrium is reached and remained constant. Namely, the removal rates for both cations were obviously faster at initial stage. The fast removal rate at the initial stage was due to the fact that, initially, all adsorbent sites were vacant and the solute concentration gradient was high [21]. Over EMRZ15, Ni^{2+} adsorption immediately took place within the first 60 min, and then reached adsorption equilibrium, demonstrating that the EMRZ15 has a strong ability for binding Ni^{2+} cations. Unlike the case of Ni^{2+} adsorption, EMRZ15 still exhibited modest increases in the Mn^{2+} uptake even after 60 min, suggesting a

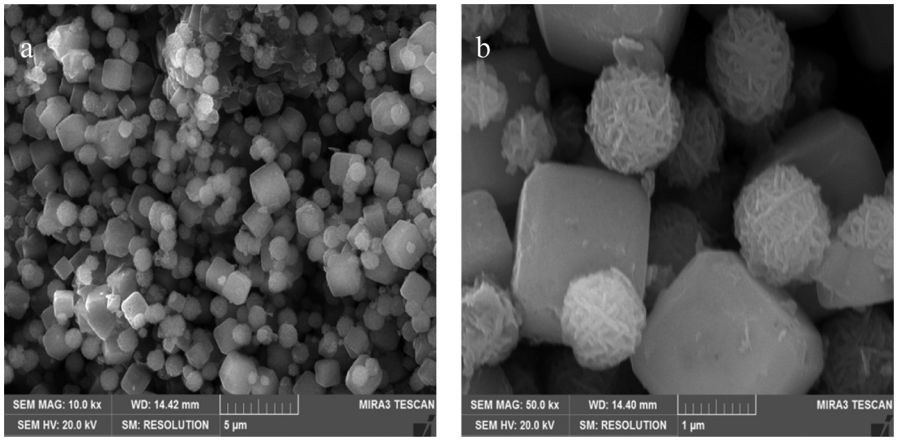

Fig. 4. SEM photomicrographs of sample EMRZ15.

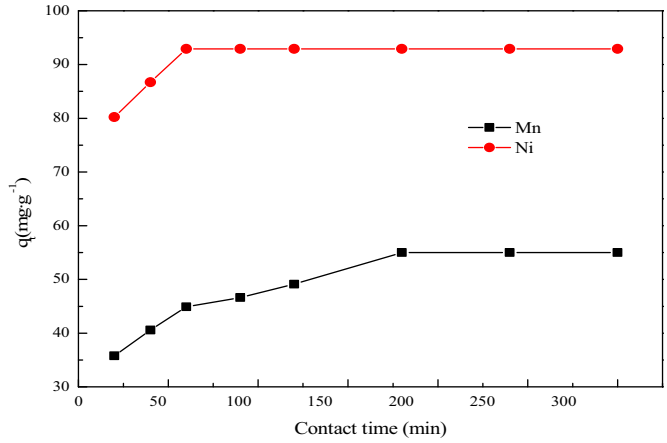

Fig. 5. Effect of contact time on heavy metal adsorption (initial metal ions concentration = 300 mg L^{-1}; adsorbent dose = 0.3 g/100 mL; pH value = 6.0; temperature = 30 °C).

slower adsorption rate than that for Ni^{2+} adsorption. This could be attributed to the larger ionic radius of Mn^{2+} that will pass with difficulty through the channels for zeolite [2,39]. And 180 min after initial reaction, the uptake amount of Mn^{2+} became almost stable at 30 °C. Thus, a contact time of 180 min was found to be sufficient for all metal studied to achieve uptake equilibrium, and the contact time was fixed at 180 min for the following batch experiments.

3.2.2. Effect of initial concentration

The effect of the initial concentration on the retention of metal ions, at concentration levels ranging from 100 to 600 mg L^{-1}, was studied at 30 °C while keeping all other parameters constant. The results are shown in Fig. 6. As can be seen from Fig. 6, it is evident that the adsorption capacity increased with an increase in the initial concentration. The increases of heavy metal adsorption with an increasing initial concentration have been widely observed in many studies [3,40]. And the figure also shows that the adsorption of the heavy metal ions at different concentrations is increased firstly and then kept increasing gradually until the equilibrium is reached and remained constant. This behavior can be explained by the fact that under higher initial concentration, more metal ions are left un-adsorbed in solution due to the saturation of binding sites [40]. These results indicate that energetically less favorable sites become involved when the concentration of metal in solution increases [8,40,41]. The heavy metal uptake is attributed to different mechanisms of ion-exchange processes as well as to the adsorption process. In this case, ICP analyses of the test solution recovered after the equilibrium adsorption revealed that the leaching amount of Na^+ was predominately enhanced in that case. This result unambiguously indicates that the uptake of metal ions proceeds via an ion-exchange mechanism, i.e., the weakly bonded, network-modifying Na^+ ions are released to the solution so as to replace with heavy metal ions. During the ion exchange process, diffusion was faster through the pores and was retarded when the ions moved through the smaller diameter channels.

3.2.3. Effect of pH

The pH of the aqueous solution is an important operational parameter in the adsorption process because it affects the solubility of the metal ions, concentration of the counter ions on the functional groups of the adsorbent and the degree of ionization of the adsorbate during reaction [40,42]. As we know, at pH value higher than 6.0, most of the heavy metal ions tend to form precipitation as hydroxides. And the "true" adsorption capacity of EMRZ15 could be masked by precipitation [43]. Thus, the adsorption of heavy metal onto EMRZ15 at pH value ranging from 1.0 to 6.0 was studied as shown in Fig. 7. From Fig. 7, an increase in pH corresponds to an increase in adsorption, reaching the maximum capacity at a pH of about 6.0. The lower adsorption of heavy metal at acidic pH is probably due to the following reasons. At lower pH values, where the concentration of H^+ is high, the competition by the negative sites on the zeolite surface is enhanced and the metal sorption is reduced accordingly [40,44]. In addition, zeolite crystals begin to collapse or dissolve with decreasing pH in aqueous solutions, particularly when the pH is below 4.0 [21]. Meanwhile, these results are in agreement with the results previously reported [40,43,44].

3.2.4. Adsorption kinetics

The kinetics of sorption of metal ions by EMRZ15 was studied for its possible importance in treatment of metal-bearing industrial effluents. In the present study, pseudo-first-order and

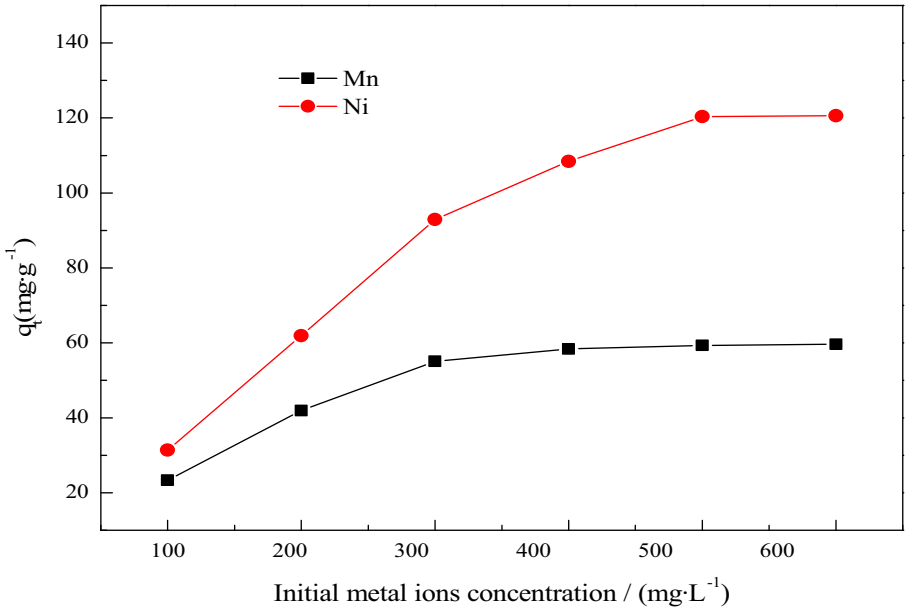

Fig. 6. Effect of initial concentration on heavy metal adsorption (contact time = 180 min; adsorbent dose = 0.3 g/100 mL; pH value = 6.0; temperature = 30 °C).

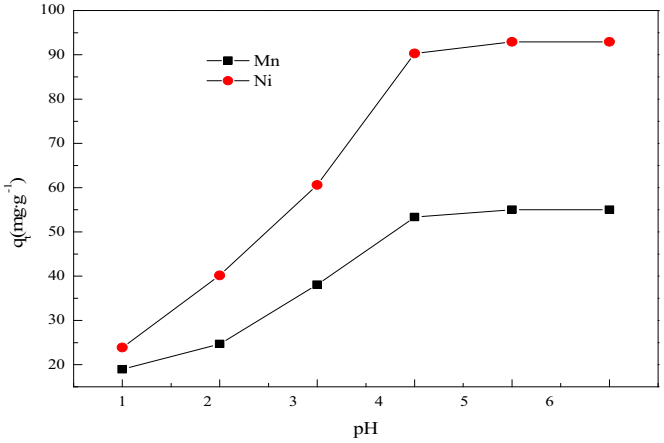

Fig. 7. Effect of pH value on heavy metal adsorption (initial metal ions concentration = 300 mg L^{-1}; contact time = 180 min; adsorbent dose = 0.3 g/100 mL; temperature = 30 °C).

pseudo-second-order kinetic models were employed to test the experimental data [4,21]. The pseudo-first-order and pseudo-second-order models are respectively described in the following equations:

$$\ln(q_e - q_t) = \ln\ q_e - k_1 t \quad (2)$$

$$\frac{t}{q_t} = \frac{1}{k_2 q_e^2} + \frac{t}{q_e} \quad (3)$$

where q_e and q_t are the amounts of adsorbate adsorbed on the adsorbents (mg g^{-1}) at equilibrium and at time t, respectively. k_1 (min^{-1}) and k_2 (g mg^{-1} min^{-1}) are the rate constants of pseudo-first-order and pseudo-second-order models, respectively.

The kinetic data were linearized using the pseudo-first-order and pseudo-second-order models, and plotted between $\ln(q_e - q_t)$ versus t and t/q_t versus t, respectively. The constants were calculated from the slope and the intercept of the plots, and are given in Table 5 and Fig. 8. The results given in Table 5 show that, for both Mn^{2+} and Ni^{2+}, the R^2 values (R^2 = 0.8616 and 0.2901) for pseudo-first order model were much lower than those obtained using the pseudo-second-order model (R^2 = 0.9979 and 0.9998). Besides, the q_e value predicted from the second-order model is much more comparable to the experimental q_e value than that from the first-order model. Thus, the pseudo-second-order model explains the kinetic processes better.

3.2.5. Adsorption isotherm

In this work, two of the most commonly used equilibrium models, the Langmuir and Freundlich isotherms, were fitted with the experimental data to find the most suitable model [5,21].

Langmuir's isotherm model suggests that uptake occurs on homogeneous surface by monolayer sorption without interaction between sorbed molecules. The linear form of Langmuir's isotherm model is given by the following equation:

$$\frac{C_e}{q_e} = \frac{1}{q_0 K_L} + \frac{C_e}{q_0} \quad (4)$$

where K_L is the adsorption equilibrium constant (L mg^{-1}), q_0 is the maximum monolayer adsorption capacity, and q_e is the amount adsorbed on a unit mass of the adsorbent (mg g^{-1}) when the equilibrium concentration is C_e (mg L^{-1}). The isotherm experimental data, which were collected at different initial metal ion concentrations, were plotted between C_e/q_e versus C_e (Fig. 9a). As seen in Fig. 9a, a linear plot is obtained when C_e/q_e is plotted against C_e over the entire concentration range of metal ions investigated. The Langmuir model parameters and the statistical fits of the sorption data to this equation are given in Table 6. Regression values (R^2) presented in Table 6 indicated that the adsorption data for heavy metal ions removal fitted well the Langmuir isotherm. Meanwhile, the extremely high value of correlation coefficient (R^2 > 0.99) for the Langmuir isotherm predicts the monolayer coverage of metal ions on EMRZ15 particles. As can be seen from the q_0 results (Table 2), Ni^{2+} adsorption was higher than Mn^{2+} adsorption for EMRZ15. The adsorption capacity of zeolites generally depends on: (1) the charge density of cations, (2) the exchangeable sites and pore size on the zeolite framework, (3) the equilibrium temperature [45–47]. Since the ion exchange was conducted at the same condition for each heavy metal species, the different adsorption capacity of cations was ascribed to the different charge density of cations. The charges of the metal cation are the same (+2); therefore charge density for Ni^{2+} ions is higher than for that of Mn^{2+}, since Ni^{2+} has lower ionic radius than that of Mn^{2+}. This difference leads Ni^{2+} to be attracted to the surface of zeolite more strongly than Mn^{2+} [46,47].

One of the essential characteristics of the Langmuir equation could be expressed in terms of a dimensionless separation factor (R_L). And R_L is defined as follows [48]:

$$R_L = \frac{1}{(1 + K_L C_0)} \quad (5)$$

where C_0 is the highest initial solute concentration (mg L^{-1}), K_L is the Langmuir's adsorption constant (L mg^{-1}). The R_L value implies the adsorption to be unfavorable (R_L > 1), linear (R_L = 1), favorable (0 < R_L < 1) or irreversible (R_L = 0). For C_0 from 50 to 250 mg L^{-1} used in the present study, the values of R_L range from 0.036 to 0.29 for Mn^{2+} and 0.023 to 0.11 for Ni^{2+}. The adsorption of Mn^{2+} and Ni^{2+} onto EMRZ15 can thus be considered favorable. In other words, the prepared EMRZ15 is a suitable sorbent for both Mn^{2+} and Ni^{2+}.

Meanwhile, the results of metal ion sorption onto EMRZ15 were also analyzed using the Freundlich model to evaluate parameters associated to the sorption behavior. The Freundlich isotherm is an empirical equation employed to describe heterogeneous systems. The linear form of Freundlich's isotherm model is expressed by the following equation:

$$\ln(q_e) = \frac{1}{n}\ln(C_e) + \ln(K_F) \quad (6)$$

where K_F ((mg g^{-1})(L g^{-1})^n) and $1/n$ are Freundlich constants related to sorption capacity and sorption intensity of adsorbents. C_e and q_e are same to those in the Langmuir isotherm model.

Freundlich isothermal plots are presented in Fig. 9b, and the Freundlich constants are also listed in Table 6. As can be seen in Fig. 9b and Table 6, the Freundlich model does not fit the data of both Mn^{2+} and Ni^{2+}, as indicated by the values of R^2 of 0.8293 and 0.7583 for Mn^{2+} and Ni^{2+}, respectively. Namely, the Langmuir isotherm

Table 5
The constants and correlation coefficients of pseudo-first order and pseudo-second order kinetic models for adsorption of heavy metal onto EMRZ15.

Metal	C_0/mg L^{-1}	q_e(exp)[a]/mg g^{-1}	Pseudo-first-order model			Pseudo-second-order model		
			q_e[a]/mg g^{-1}	k_1/min^{-1}	R^2	q_e[a]/mg g^{-1}	k_2/g mg^{-1} min^{-1}	R^2
Mn^{2+}	300	55.03	64.23	0.03293	0.8616	58.62	0.001091	0.9979
Ni^{2+}	300	92.91	0.7213	0.01966	0.2901	93.73	0.005668	0.9998

[a] q_e(exp) and q_e are the experimental and calculated values of q_e, respectively.

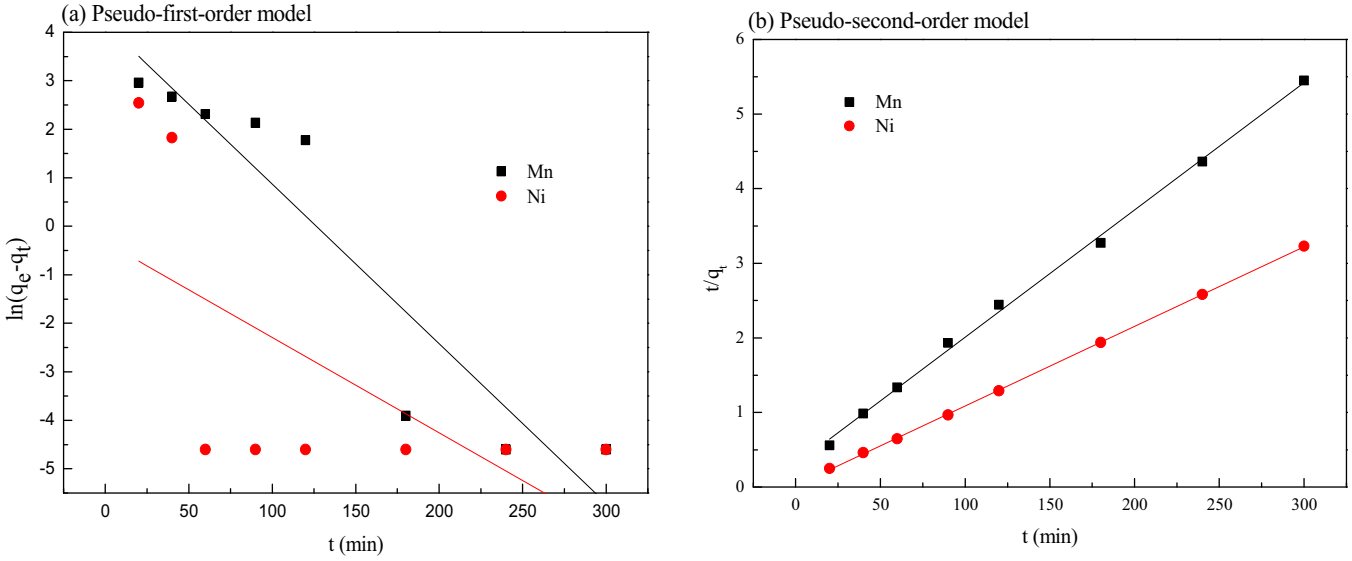

Fig. 8. Plots of kinetics of heavy metal removal by the EMRZ15 (initial metal ions concentration = 300 mg L^{-1}; adsorbent dose = 0.3 g/100 mL; pH value = 6.0; temperature = 30 °C).

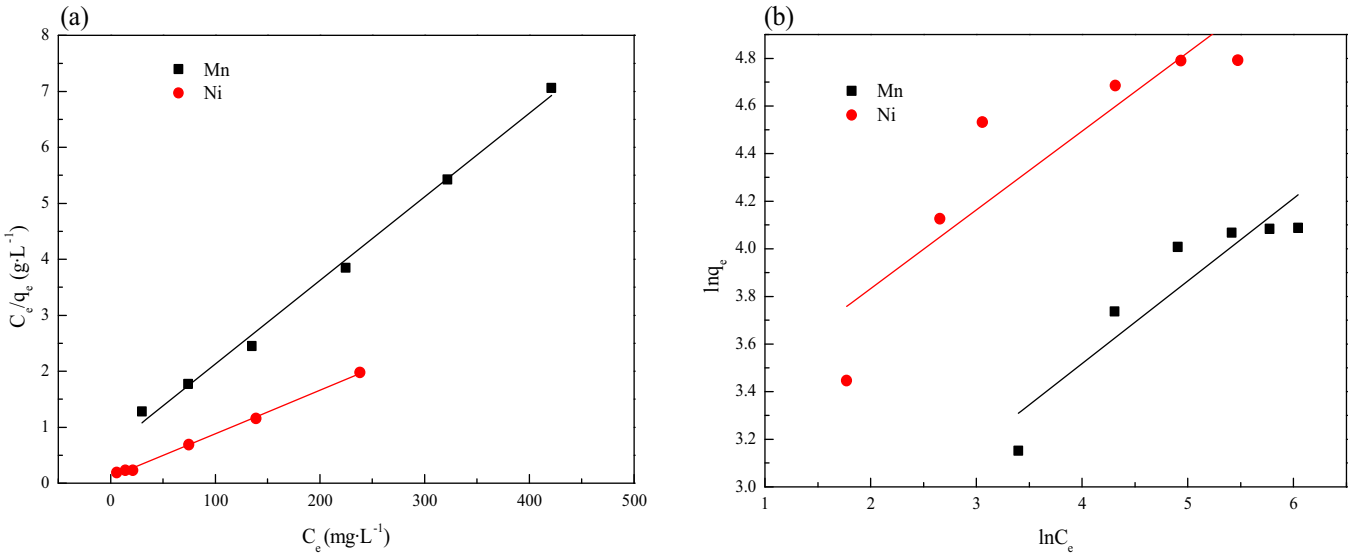

Fig. 9. (a) Langmuir and (b) Freundlich isotherm adsorption model of the Mn^{2+} or Ni^{2+} onto EMRZ15 (adsorbent dose = 0.3 g/100 mL; contact time = 180 min; pH value = 6.0; temperature = 30 °C).

model fits the experimental data better compared to the Freundlich model. Consequently, the sorption of metal ions on EMRZ15 follows the Langmuir isotherm model where the uptake occurs on homogeneous surface by monolayer sorption without interaction between sorbed ions [48].

3.3. Comparison between our results and related literature

Table 7 lists the comparison of maximum adsorption capacity of Mn^{2+} and Ni^{2+} on various adsorbents. For Mn^{2+}, the EMRZ15 has a greater capacity than natural clinoptilolite [8], natural zeolite [49], vermiculite [50], and Na-montmorillonite [51]. For Ni^{2+}, the adsorption capacity of EMRZ is much higher than other low-cost adsorbents such as spirodela intermedia, Brazilian natural scolecite, pretreated clinoptilolite, natural bentonite, vermiculite and Na-montmorillonite [5,7,44,50–52]. Thus, it is evident that EMRZ15 shows great potential as an adsorbent for meatal ions. Besides, the adsorption of Mn^{2+} and Ni^{2+} onto standard zeolites (zeolite A, Y and P) was conducted in order to investigate which component is responsible for the superior performance

Table 6
Parameters of adsorption isotherms of heavy metal onto EMRZ15 at 30 °C.

Metal	pH	Langmuir isotherm			Freundlich isotherm		
		K_L (L mg^{-1})	q_0 (mg g^{-1})	R^2	K_F (mg g^{-1})(L g^{-1})^n	$1/n$	R^2
Mn^{2+}	6.0	0.02373	66.93	0.9942	8.421	0.3468	0.8293
Ni^{2+}	6.0	0.07380	128.70	0.9977	23.834	0.3305	0.7583

Table 7
Comparison of maximum adsorption capacity of metal ions on various adsorbents.

	Adsorbent	q_0 (mg g^{-1})	Reference
Ni^{2+}	EMRZ15	128.70	This work
	Spirodela intermedia	122.10	[5]
	Pretreated clinoptilolite	15.55	[7]
	Brazilian natural scolecite	3.52	[44]
	Vermiculite	25.33	[50]
	Na-montmorillonite	3.63	[51]
	Natural bentonite	4.27	[52]
Mn^{2+}	EMRZ15	66.93	This work
	Natural clinoptilolite	4.22	[8]
	Natural Turkish zeolite	2.42	[49]
	Vermiculite	26.78	[50]
	Na-montmorillonite	3.22	[51]

of the EMRZ15, since the synthesized EMRZ15 was a mixture of zeolites (see Fig. 2). And the tests were made under following conditions: initial metal ions concentration = 300 mg L^{-1}; adsorbent dose = 0.3 g/100 mL; pH value = 6.0; temperature = 30 °C; contact time = 180 min. It was found that the uptake capacity for Ni^{2+} and Mn^{2+} by commercially available zeolite A, P and Y were determined to be 108.57, 80.86, 56.62 mg g^{-1} and 65.59, 48.26, 35.42 mg g^{-1}, respectively. Hence, compared to the adsorption capacity of Mn^{2+} and Ni^{2+} by EMRZ15 under the same condition (see Fig. 5), it could be stated that the zeolite A in EMRZ15 plays the main role in the Mn^{2+} and Ni^{2+} uptake. This statement is also supported by the results from XRD analysis (Fig. 2) showing that Na-A zeolite was the major constituent of EMRZ15.

4. Conclusions

In the present study, we have first reported on the synthesis of zeolite utilizing EMR as an abundant and cheap chemical source from the viewpoint of the chemical and economical use of EMR. Analyses by means of XRD, FT-IR, FE-SEM, XRF, CEC and BET surface area measurement indicated that the zeolite synthesized at Si/Al ratio = 1.5, namely EMRZ15, was mainly composed of Na-A zeolite and the zeolite material has specific properties such as high purity and CEC. The adsorption of Mn^{2+} and Ni^{2+} was found to be dependent on initial concentration, pH and contact time. The adsorbed amount of Mn^{2+} and Ni^{2+} both increased with increasing initial concentration, pH and contact time. Langmuir isotherm displayed a better fitting model than Freundlich isotherm, thus, indicating to the applicability of monolayer coverage of metal ions on the surface of adsorbent. The kinetic process can be predicted by pseudo-second-order model and rate constants for Mn^{2+} and Ni^{2+} sorption were found to be 0.001091 and 0.005668 g mg^{-1} min^{-1}, respectively at 30 °C. Moreover, the maximum sorption capacities for Mn^{2+} and Ni^{2+} shown by EMRZ15 were 66.93 mg g^{-1} and 128.70 mg g^{-1}, respectively. These results show that EMRZ15 is a highly efficient adsorbent for metal ions removal from aqueous solution, which exhibits much higher adsorption capacity than other low-cost adsorbents. This conversion process, which enables us to fabricate valuable zeolite materials from EMR at low cost and through convenient preparation steps, is surely beneficial from the viewpoint of the chemical and economical use of EMR.

Acknowledgments

The authors are grateful for the National Natural Science Foundation of China (No.21376273) and the Major Project of Science and Technology of Hunan Province (No.2010FJ1011) by offering the research fund.

References

[1] Z. Elouear, J. Bouzid, N. Boujelben, M. Feki, F. Jamoussi, A. Montiel, Heavy metal removal from aqueous solutions by activated phosphate rock, J. Hazard. Mater. 156 (2008) 412–420.
[2] T.S. Jamil, H.S. Ibrahim, I.H. Abd El-Maksoud, S.T. El-Wakeel, Application of zeolite prepared from Egyptian kaolin for removal of heavy metals: I. Optimum conditions, Desalination 258 (2010) 34–40.
[3] M. Prasad, H.Y. Xu, S. Saxena, Multi-component sorption of Pb (II), Cu (II) and Zn (II) onto low-cost mineral adsorbent, J. Hazard. Mater. 154 (2008) 221–229.
[4] F. Pagnanelli, S. Mainelli, F. Vegliò, L. Toro, Heavy metal removal by olive pomace: biosorbent characterization and equilibrium modelling, Chem. Eng. Sci. 58 (2003) 4709–4717.
[5] P. Miretzky, A. Saralegui, A.F. Cirelli, Simultaneous heavy metal removal mechanism by dead macrophytes, Chemosphere 62 (2006) 247–254.
[6] R. Petrus, J.K. Warchol, Heavy metal removal by clinoptilolite. An equilibrium study in multi-component systems, Water Res. 39 (2005) 819–830.
[7] M. Sprynskyy, B. Buszewski, A.P. Terzyk, J. Namiesnik, Study of the selection mechanism of heavy metal (Pb^{2+}, Cu^{2+}, Ni^{2+}, and Cd^{2+}) adsorption on clinoptilolite, J. Colloid Interface Sci. 304 (2006) 21–28.
[8] M. Kobya, E. Demirbas, E. Senturk, M. Incea, Adsorption of heavy metal ions from aqueous solutions by activated carbon prepared from apricot stone, Bioresour. Technol. 96 (2005) 1518–1521.
[9] K. Hagelstein, Globally sustainable manganese metal production and use, J. Environ. Manage. 90 (2009) 3736–3740.
[10] N. Duan, Z. Dan, F. Wang, C.X. Pan, C.B. Zhou, L.H. Jiang, Electrolytic manganese metal industry experience based China's new model for cleaner production promotion, J. Clean. Prod. 19 (2011) 2082–2087.
[11] C.X. Li, H. Zhong, S. Wang, J.R. Xue, Leaching behavior and risk assessment of heavy metals in a landfill of electrolytic manganese residue in Western Hunan, China, Hum. Ecol. Risk. Assess. 20 (2014) 1249–1263.
[12] N. Hu, J.F. Zheng, D.X. Ding, J. Liu, L.Q. Yang, J. Yin, G.Y. Li, Y.D. Wang, Y.L. Liu, Metal pollution in Huayuan River in Hunan Province in China by manganese sulphate waste residue, Bull. Environ. Contam. Toxicol. 83 (2009) 583–590.
[13] D. Qiao, J.S. Qian, Q.Z. Wang, Y.D. Dang, H. Zhang, D.Q. Zeng, Utilization of sulfate-rich solid wastes in rural road construction in the Three Gorges Reservoir, Resour. Conserv. Recy. 54 (2010) 1368–1376.
[14] Z.G. Zhou, L.J. Xu, J.L. Xie, C.L. Liu, Effect of manganese tailings on capsicum growth, Chin. J. Geochem. 28 (2009) 427–431.
[15] J. Wang, B. Peng, L.Y. Chai, Q. Zhang, Q. Liu, Preparation of electrolytic manganese residue–ground granulated blastfurnace slag cement, Powder Technol. 241 (2013) 12–18.
[16] P.K. Hou, J.S. Qian, Z. Wang, C. Deng, Production of quasi-sulfoaluminate cementitious materials with electrolytic manganese residue, Cem. Concr. Compos. 34 (2012) 248–254.
[17] J. Peric, M. Trgo, N.V. Medvidovic, Removal of zinc, copper and lead by natural zeolite—a comparison of adsorption isotherms, Water Res. 38 (2004) 1893–1899.
[18] S.B. Wang, Y.L. Peng, Natural zeolites as effective adsorbents in water and wastewater treatment, Chem. Eng. J. 156 (2010) 11–24.
[19] S.K. Pitcher, R.C.T. Slade, N.I. Ward, Heavy metal removal from motorway stormwater using zeolites, Sci. Total Environ. 334–335 (2004) 161–166.
[20] C.X. Li, H. Zhong, S. Wang, J.R. Xue, Z.Y. Zhang, Removal of basic dye (methylene blue) from aqueous solution using zeolite synthesized from electrolytic manganese residue, J. Ind. Eng. Chem. (2014), http://dx.doi.org/10.1016/j.jiec.2014.08.038.
[21] M.L. Zhang, H.Y. Zhang, D. Xu, L. Han, D.X. Niu, B.H. Tian, J. Zhang, Y. Zhang, W.S. Wu, Removal of ammonium from aqueous solutions using zeolite synthesized from fly ash by a fusion method, Desalination 271 (2011) 111–121.
[22] C. Belviso, F. Cavalcante, S. Fiore, Synthesis of zeolite from Italian coal fly ash: differences in crystallization temperature using seawater instead of distilled water, Waste Manage. 30 (2010) 839–847.
[23] Y. Kuwahara, T. Ohmichi, T. Kamegawa, K. Mori, H. Yamashita, A novel conversion process for waste slag: synthesis of a hydrotalcite-like compound and zeolite from blast furnace slag and evaluation of adsorption capacities, J. Mater. Chem. 20 (2010) 5052–5062.
[24] M. Nascimento, P.S.M. Soares, V.P. Souza, Adsorption of heavy metal cations using coal fly ash modified by hydrothermal method, Fuel 88 (2009) 1714–1719.
[25] R.M. Mohamed, A.A. Ismail, G. Kini, I.A. Ibrahim, B. Koopman, Synthesis of highly ordered cubic zeolite A and its ion-exchange behavior, Colloids Surf. A 348 (2009) 87–92.
[26] R. Terzano, M. Spagnuolo, L. Medici, F. Tateo, P. Ruggiero, Zeolite synthesis from pre-treated coal fly ash in presence of soil as a tool for soil remediation, Appl. Clay Sci. 29 (2005) 99–110.
[27] L.C. Peng, D.Y. Wu, Y.M. Sui, X. Shang, X.Y. Zheng, H.N. Kong, Effect of competitive cations on the removal of ammonium by zeolite synthesized from coal fly ash, Environ. Sci. Technol. 33 (2010) 146–149.
[28] H. Kazemian, Z. Naghdali, T. Ghaffari Kashani, F. Farhadi, Conversion of high silicon fly ash to Na-P1 zeolite: alkaline fusion followed by hydrothermal crystallization, Adv. Powder. Technol. 21 (2010) 279–283.
[29] L. Liu, R. Singh, P. Xiao, P.A. Webley, Y. Zhai, Zeolite synthesis from waste fly ash and its application in CO_2 capture from flue gas streams, Adsorption 17 (2011) 795–800.

[30] A. Medina, P. Gamero, J.M. Almanza, A. Vargas, A. Montoya, G. Vargas, M. Izquierdo, Fly ash from a Mexican mineral coal. II. Source of W zeolite and its effectiveness in arsenic (V) adsorption, J. Hazard. Mater. 181 (2010) 91–104.
[31] K.M. Lee, Y.M. Jo, Synthesis of zeolite from waste fly ash for adsorption of CO_2, J. Mater. Cycles Waste Manage. 12 (2010) 212–219.
[32] N. Koukouzasa, C. Vasilatos, G. Itskos, I. Mitsisb, A. Moutsatsou, Removal of heavy metals from wastewater using CFB-coal fly ash zeolitic materials, J. Hazard. Mater. 173 (2010) 581–588.
[33] R. Juan, S. Hernández, J.M. Andrés, C. Ruiz, Ion exchange uptake of ammonium in wastewater from a sewage treatment plant by zeolitic materials from fly ash, J. Hazard. Mater. 161 (2009) 781–786.
[34] D. Karadag, Y. Koc, M. Turan, B. Armagan, Removal of ammonium ion from aqueous solution using natural Turkish clinoptilolite, J. Hazard. Mater. 136 (2006) 604–609.
[35] H.M. Huang, X.M. Xiao, B. Yan, L.P. Yang, Ammonium removal from aqueous solutions by using natural Chinese (Chende) zeolite as adsorbent, J. Hazard. Mater. 175 (2010) 247–252.
[36] N.M. Musyoka, L.F. Petrik, E. Hums, H. Baser, W. Schwieger, In situ ultrasonic monitoring of zeolite A crystallization from coal fly ash, Catal. Today 190 (2012) 38–46.
[37] S. Alfaro, C. Rodríguez, M.A. Valenzuela, P. Bosch, Aging time effect on the synthesis of small crystal LTA zeolites in the absence of organic template, Mater. Lett. 61 (2007) 4655–4658.
[38] M. Alkan, C. Hopa, Z. Yilmaz, H. Güler, The effect of alkali concentration and solid/liquid ratio on the hydrothermal synthesis of zeolite NaA from natural kaolinite, Microporous Mesoporous Mater. 86 (2005) 176–184.
[39] H.K. An, B.Y. Park, D.S. Kim, Crab shell for the removal of heavy metals from aqueous solution, Water Res. 35 (2001) 3551–3556.
[40] O.S. Amuda, A.A. Giwa, I.A. Bello, Removal of heavy metal from industrial wastewater using modified activated coconut shell carbon, Biochem. Eng. J. 36 (2007) 174–181.
[41] M. Al-Anber, Z.A. Al-Anber, Utilization of natural zeolite as ion-exchange and sorbent material in the removal of iron, Desalination 225 (2008) 70–81.
[42] A. Aklil, M. Mouflih, S. Sebti, Removal of heavy metal ions from water by using calcined phosphate as a new adsorbent, J. Hazard. Mater. A 112 (2004) 183–190.
[43] S. Kocaoba, Y. Orhan, T. Akyüz, Kinetics and equilibrium studies of heavy metal ions removal by use of natural zeolite, Desalination 214 (2007) 1–10.
[44] S.M.D. Bosco, R.S. Jimenez, W.A. Carvalho, Removal of toxic metals from wastewater by Brazilian natural scolecite, J. Colloid Interface Sci. 281 (2005) 424–431.
[45] W. Qiu, Y. Zheng, Removal of lead, copper, nickel, cobalt, and zinc from water by a cancrinite-type zeolite synthesized from fly ash, Chem. Eng. J. 145 (2009) 483–488.
[46] R. Shawabkeh, A. Al-Harahsheh, M. Hami, A. Khlaifat, Conversion of oil shale ash into zeolite for cadmium and lead removal from wastewater, Fuel 83 (2004) 981–985.
[47] E. Erdem, N. Karapinar, R. Donat, The removal of heavy metal cations by natural zeolites, J. Colloid Interface Sci. 280 (2004) 309–314.
[48] V.B.H. Dang, H.D. Doan, T. Dang-Vu, A. Lohi, Equilibrium and kinetics of biosorption of cadmium (II) and copper (II) ions by wheat straw, Bioresour. Technol. 100 (2009) 211–219.
[49] T. Motsi, N.A. Rowson, M.J.H. Simmons, Adsorption of heavy metals from acid mine drainage by natural zeolite, Int. J. Miner. Process. 92 (2009) 42–48.
[50] M. Malandrinoa, O. Abollinoa, A. Giacominoa, M. Acetob, E. Mentasti, Adsorption of heavy metals on vermiculite: influence of pH and organic ligands, J. Colloid Interface Sci. 299 (2006) 537–546.
[51] O. Abollino, M. Aceto, M. Malandrino, C. Sarzanini, E. Mentasti, Adsorption of heavy metals on Na-montmorillonite. Effect of pH and organic substances, Water Res. 37 (2003) 1619–1627.
[52] R. Donat, A. Akdogan, E. Erdem, H. Cetisli, Thermodynamics of Pb^{2+} and Ni^{2+} adsorption onto bentonite from aqueous solutions, J. Colloid Interface Sci. 286 (2005) 43–52.